1 **Characterizing Charge Structure in Central Argentina Thunderstorms**

2 **During RELAMPAGO Utilizing a New Charge Layer Polarity Identification**

3 **Method**

4 **Bruno L. Medina[1], Lawrence D. Carey[1], Timothy J. Lang[2], Phillip M. Bitzer[1], Wiebke**

5 **Deierling[3], and Yanan Zhu[4]**

6 [1]Department of Atmospheric and Earth Science, The University of Alabama in Huntsville,
7 Huntsville, AL, USA.

8 [2]NASA Marshall Space Flight Center, Huntsville, AL, USA.

9 [3]University of Colorado Boulder, Boulder, CO, USA.

10 [4]Earth System Science Center, The University of Alabama in Huntsville, Huntsville, AL, USA.

11 Corresponding author: Bruno Medina (blm0032@uah.edu)

12 **Key Points:**

13 • A new automated method to estimate the polarity, altitude, and vertical depth of charge
14   layers from flashes is presented.

15 • Thunderstorm charge structures in Central Argentina are characterized from months of
16   LMA data, with 13.3% anomalous charge structure.

17 • Cordoba anomalously charged thunderstorms have a distinct charge altitude distribution
18   when compared to those in Colorado.

Abstract

A new automated method to retrieve charge layer polarity from flashes, named Chargepol, is presented in this paper. Using data from the NASA Lightning Mapping Array (LMA) deployed during the RELAMPAGO field campaign in Cordoba, Argentina, from November 2018 to April 2019, this method estimates the polarity of vertical charge distributions and their altitudes and thicknesses (or vertical depth) using the very-high frequency (VHF) source emissions detected by LMAs. When this method is applied to LMA data for extended periods of time, it is capable of inferring a storm's bulk electrical charge structure throughout its life cycle. This method reliably predicted the polarity of charge within which lightning flashes propagated and was validated in comparison to methods that require manual assignment of polarities via visual inspection of VHF lightning sources. Examples of normal and anomalous charge structures retrieved using Chargepol for storms in Central Argentina during RELAMPAGO are presented for the first time. Application of Chargepol to five months of LMA data in Central Argentina and several locations in the United States allowed for the characterization of the charge structure in these regions and for a reliable comparison using the same methodology. About 13.3% of Cordoba thunderstorms were defined by an anomalous charge structure, slightly higher than in Oklahoma (12.5%) and West Texas (11.1%), higher than Alabama (7.3%), and considerably lower than in Colorado (82.6%). Some of the Cordoba anomalous thunderstorms presented enhanced low-level positive charge, a feature rarely if ever observed in Colorado thunderstorms.

1 Introduction

Past studies have associated the severity of thunderstorms with patterns in charge distribution (Wiens et al., 2005; Fuchs et al., 2018). The dominant meteorological environment provides initial conditions that would influence the kinematics and microphysics within thunderstorms, which in turn affects its charge structure and dominant cloud-to-ground lightning (CG) polarity. Relatively few studies have documented the charge structure over continents other than North America (Lopez et al., 2019; Pawar & Kamra, 2004; Pineda et al., 2016; Qie et al., 2005). Furthermore, documenting charge structure in regions such as Argentina, which has perhaps some of the highest flash rate thunderstorms in the world (Zipser et al., 2006), is crucial for understanding such understudied thunderstorms.

Due to the nature of lightning processes and their characteristic emission in the VHF spectrum, thunderstorm charge structures associated with flashes can be inferred from Lightning Mapping Array (LMA) observations (Lang & Rutledge, 2011; Rust et al., 2005; Wiens et al., 2005). Based on knowledge of radiation propagation by lightning, VHF-based sensors primarily detect radiation from negative breakdown of lightning that propagates through regions of positive charge (Mazur & Ruhnke, 1993; Rison et al., 1999). Then, mapping of VHF sources is used to manually determine the location of positive and negative charge layers (Bruning et al., 2007; Lang and Rutledge, 2008; Rust et al., 2005; Wiens et al., 2005). An intra-cloud lightning (IC) flash initiates in a region with strong electric field, in between regions of charge with opposite polarities. Upon initiation, bi-direction leaders are formed and move into opposite regions of charge: a positive leader moves to a region of net negative charge, and a negative leader moves to a region of positive charge in the cloud (Coleman et al., 2003; Kasemir, 1960). When a leader reaches a charge layer, it propagates horizontally through the charge layer away from the flash initiation location (Shao & Krehbiel, 1996). Flashes propagating through charge regions that constitute a vertical dipole with positive charge located above negative charge, are

referred to as positive cloud flashes (+IC), while flashes that propagate through negative over positive dipoles are defined as negative cloud flashes (-IC, Bruning et al., 2014). K-processes may also occur, transporting charge to the base of the initial channel (Shao & Krehbiel, 1996). Observations of the VHF altitude source distributions for long periods of time are generally used to infer the location of charge regions, as the altitude with most sources are often associated with positive charge layers (Fuchs et al., 2018; Fuchs & Rutledge 2018; Lang et al., 2020; Lang & Rutledge, 2011). Tessendorf et al. (2007b) infer charge layer polarity automatically by using the first LMA source altitude for a flash, and the number of sources above and below that altitude. Stough and Carey (2020) utilized the DBSCAN (Density-Based Spatial Clustering of Applications with Noise, Ester et al., 1996) algorithm to identify regions of dense sources and infer charge region polarity. Electric field soundings have been deployed to infer polarity of charge regions within and nearby thunderstorms (Marshall et al., 1995; Rust & MacGorman, 2002; Stolzenburg et al., 1998), and have been compared to LMA-inferred charge regions (Rust et al., 2005). In order to interpret an electric field dataset with altitude, the Gauss' Law approximation is assumed, where the charge density is proportional to the electric field variation with height (Stolzenburg et al., 1998).

In order for clouds to build regions of net charge polarity and become electrified, the non-inductive charging (NIC) mechanism is thought to dominate, which does not require a pre-existing electric field to polarize the cloud and precipitation size particles. In the NIC mechanism, the polarity that graupel particles acquire when colliding with ice crystals in the presence of supercooled liquid water (Saunders et al., 1991; Takahashi, 1978) depends on the temperature, and the effective liquid water content (EWC, the accreted fraction of the liquid water content). High (low) temperature and large (small) EWC are associated with graupel charging positively (negatively), and ice crystals charging negatively (positively) (Berdeklis & List, 2001; Pereyra et al., 2000; Saunders et al., 1991, 2001; Saunders & Peck, 1998; Takahashi, 1978). As the rimer particle (e.g., graupel) accretes supercooled liquid water, it is heated by latent heat, which sublimates the ice surface and reduces the diffusional growth (Williams et al., 1991). According to the relative diffusional growth theory (Baker et al., 1987; Emersic & Saunders, 2010), the ice particle growing faster by diffusion acquires positive charge. Particle differential fall speeds and updrafts lead to storm-scale charge separation, with ice crystals being transported upward to cloud tops, and graupel residing in the mixed-phase region in the mid-levels forming the two largest charge regions during the developing-to-mature stage of thunderstorms (Williams, 1985).

Thunderstorms with upper-level negative and mid-level positive charge layers define an anomalous charge structure, as observed in thunderstorms during the STEPS field campaign conducted in Kansas, Colorado, and Nebraska (MacGorman et al., 2005; Rust et al., 2005; Rust & MacGorman, 2002; Tessendorf et al., 2007a; Tessendorf et al., 2007b; Weiss et al., 2008; Wiens et al., 2005). They have also been observed in thunderstorms in Oklahoma by Marshall et al. (1995) and Emersic et al. (2011), during the TELEX field campaign (MacGorman et al., 2008), in Texas (Chmielewski et al., 2018), Alabama (Stough & Carey, 2020), and Spain (Pineda et al., 2016). Storms with a normal charge structure would have a dominant net negative charge in the mixed-phase layer, and net positive above, as demonstrated in early foundational studies reviewed by Williams (1985), in the in-situ aircraft studies by Dye et al. (1986, 1988, 1989), during TELEX (Bruning et al., 2007) and STEPS (Weiss et al., 2008) field campaigns, among others. A low-level charge layer with opposite polarity to the nearest charge region is occasionally present (Lopez et al., 2019; Pawar & Kamra, 2004; Williams, 1989) and, if positive

109 and abnormally large, may also be termed anomalous (Bruning et al., 2014; Fuchs et al., 2015;
110 Qie et al., 2005). Some events can have multiple charge regions, such as mesoscale convective
111 systems (MCSs) (Lang & Rutledge, 2008; Lund et al., 2009; Stolzenburg et al., 1998), multicell
112 storms (Bruning et al., 2007), and supercells (Bruning et al., 2010; Calhoun et al., 2013; Wiens et
113 al., 2005).

114 Fuchs and Rutledge (2018) analyzed a large lightning flash dataset for isolated cells in
115 four different regions in the United States, and found that Colorado storms have a prevalence of
116 anomalous charge structures compared to other regions. Colorado's highest flash rate mode was
117 observed at lower levels (warmer temperatures and higher radar reflectivity values) than in other
118 regions. In addition, they suggested that Colorado is followed by Oklahoma in terms of
119 anomalous storm frequency, followed by Alabama and Washington D.C. with rare anomalous
120 observations. A large occurrence of positive cloud-to-ground lightning (+CG) is often associated
121 with anomalous charge structure storms, as a main net positive charge region is at the middle or
122 low levels of a storm instead of near its top, facilitating the propagation of positive leaders
123 toward the ground, especially if a small opposite (negative) charge region is present at lower
124 levels. Orville and Huffines (2001) found that the percentage of +CGs in the United States varies
125 from 2% in Florida to 10-20% in a region extending from the High Plains of Eastern Colorado to
126 the Upper Midwest. In the central and north Great Plains, a high percentage (>50%) of severe
127 storm reports were found to be associated with predominantly +CG lightning (>50% of CGs
128 being positive), when compared to southern Great Plains and eastern United States (Carey et al.,
129 2003).

130 This study aims to characterize the charge structure in the Central Argentina region for
131 the first time, utilizing a large dataset, as it is a key science goal of the RELAMPAGO (Remote
132 sensing of Electrification, Lightning, And Mesoscale/microscale Processes with Adaptive
133 Ground Observations) field campaign (Nesbitt et al., 2021). This novel research is achieved by
134 first developing and testing a new automated method to retrieve thunderstorm charge layer
135 polarity using Lightning Mapping Array (LMA) source and flash data, which is described in this
136 paper. Southeast South America has among the most severe thunderstorms in the world in terms
137 of high flash rate (Zipser et al., 2006), hail size (Cecil & Blankenship, 2012), heavy
138 precipitation, and flash floods (Rasmussen et al., 2014). Lightning characteristics have only been
139 documented using LMA data recently in this region (Lang et al., 2020), and the distribution of
140 charge within Argentina thunderstorms is explored for the first time in great detail in this study.
141 The general charge structure is estimated for a large dataset with a new algorithm, allowing for
142 the inference of the likelihood of normal and anomalous charge structure. Similar to Tessendorf
143 et al. (2007b) and Stough and Carey (2020), this method automatically infers charge polarity
144 from flashes, more closely resembling Tessendorf et al. (2007b) method but with improved
145 procedures, better emulating the steps that a human expert would perform when assigning
146 polarity to LMA sources for a flash by detecting the negative leader in a bi-directional model and
147 assigning polarity to sources of a flash (e.g., Rust et al. 2005). In this study, if a given lightning
148 flash passes a series of conditions, an algorithm analyzes its source location and time in order to
149 produce a prediction of charge layer polarity for that flash. This method has the capability to be
150 quickly applied to a large number of lightning flashes in a large LMA dataset (e.g., a few
151 minutes to process 24 hours of LMA flash level data within 100 km of the network center),
152 which allows for the inference of the general charge structure and its evolution in time for a
153 thunderstorm or for a large area of interest, as demonstrated by examples in this paper. The new
154 algorithm infers three-dimensional charge distribution on the flash level but its output is

155 simplified to vertical charge layer profiles for the science applications highlighted in this study.
156 Hence, output of this method is similar to manual assignment of polarity, providing positive and
157 negative layer altitude and vertical depth, but it is much less labor intensive. This algorithm
158 provides a detailed inference of the charge layer distribution in the vertical, including altitude
159 and vertical depth of negative charge layers, which is often not possible to be analyzed from the
160 VHF source distribution analysis, a method in which positive charge altitude is inferred from its
161 peak distribution. Lastly, this paper will present a detailed application of the new charge layer
162 polarity algorithm by characterizing the charge structure of Central Argentinian thunderstorms
163 by processing a large multi-month sample of LMA observations for the first time. The algorithm
164 performance is then further demonstrated through its application to multi-month LMA datasets
165 from several locations in the United States in which charge structure has already been
166 documented using the LMA-based charge layer retrieval techniques discussed above. The
167 additional application herein allows the charge structure of Central Argentinian thunderstorms to
168 be compared for the first time to several well-studied locations in the United States such as
169 Colorado, Oklahoma, West Texas and Alabama using the same algorithm. Consistency with
170 prior studies of charge structure in well observed regions of the United States ensures that this
171 method is applicable for future work.

2 Lightning Networks Deployed During RELAMPAGO and DC3

173 The Lightning Mapping Array (LMA) is a GPS-based network (Goodman et al., 2005;
174 Koshak et al., 2004; Krehbiel et al., 2000; Rison et al., 1999) that operates in the VHF
175 electromagnetic spectrum (Krehbiel et al., 2000), in which radiation events detected are often
176 associated with lightning breakdown processes (Rison et al., 1999). LMAs locate and report the
177 time of VHF sources emitted during lightning breakdown processes using a time-of-arrival
178 technique (Koshak et al., 2004; Koshak & Solakiewicz, 1996; Lhermitte & Krehbiel, 1979;
179 Thomas et al., 2004), where a χ^2 goodness-of-fit function with a threshold of lower than 5 is
180 utilized to minimize location errors, and minimum of 6 operating network sensors are required to
181 ensure location accuracy (Chmielewski and Bruning, 2016). The lmatools Python package
182 (Bruning et al., 2015) was used to process LMA source data into lightning flash datasets. This
183 package is based on the DBSCAN (Ester et al., 1996) algorithm, a machine learning algorithm
184 used to cluster VHF sources to reconstruct the shapes (structure) of entire lightning flashes.
185 DBSCAN randomly searches for clusters of VHF sources in space and time, and groups each
186 cluster individually. These groups are used to define individual flashes using the following
187 criteria: source-to-source minimum distance and time thresholds of 3000 meters and 150 ms,
188 respectively, and a maximum flash duration of 3 seconds (Fuchs et al., 2016).

189 As part of the RELAMPAGO field campaign (Nesbitt et al., 2021), an LMA of 11
190 sensors was deployed by NASA Marshall Space Flight Center to the eastern side of the Sierra de
191 Cordoba mountains in the province of Cordoba, Central Argentina, from mid-November 2018 to
192 mid-April 2019 (Lang et al., 2020). RELAMPAGO LMA data was used in this study for
193 development and validation of the charge layer inference method, and characterization of the
194 charge structure climatology in the Cordoba warm season. In addition, LMA datasets from the
195 DC3 (Deep Convective Clouds and Chemistry, Barth et al., 2015) field campaign are used to
196 independently estimate the charge structure in a variety of climatological regimes of the United
197 States to compare results of the presented algorithm with those of other studies, and with storms
198 in the Cordoba region of Argentina examined during RELAMPAGO. During the DC3 field
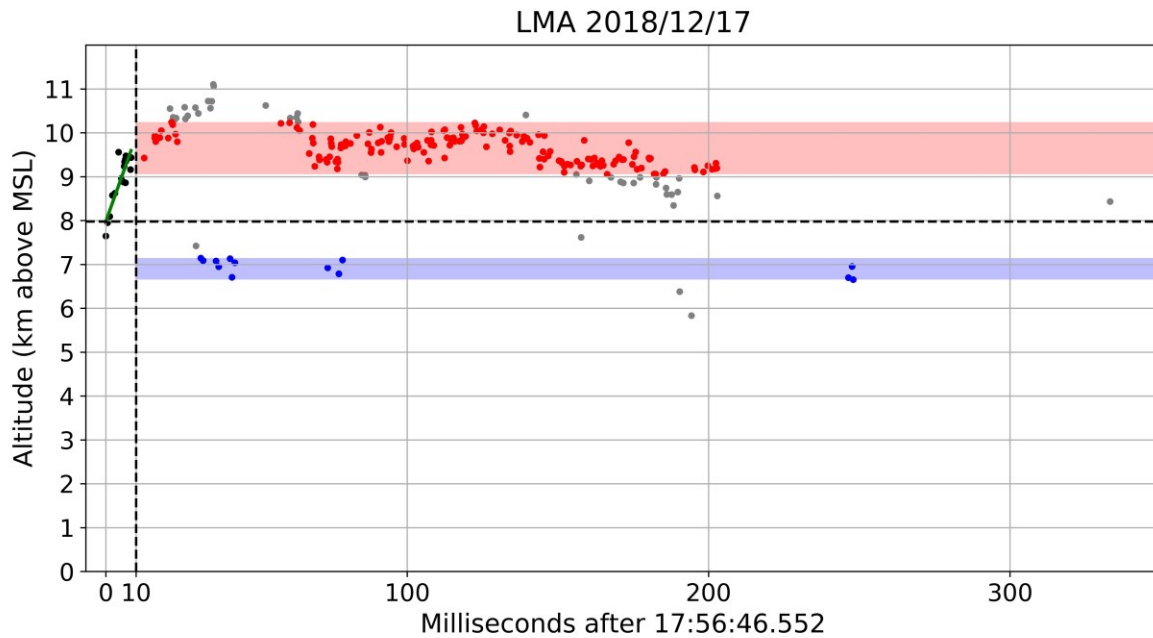199 campaign, LMA networks were deployed simultaneously in Alabama, West Texas, Oklahoma,

200 and Colorado in May and June 2012 (Barth et al., 2015; DiGangi et al., 2016; Mecikalski et al.,
201 2015). For each dataset, only flashes with centroid location within the 100 km range distance
202 from the LMA network center are being considered in this study, as altitude errors are expected
203 to be smaller and the flash detection efficiency to be higher (Chmielewski & Bruning 2016;
204 Koshak et al. 2004; Lang et al., 2020; Thomas et al. 2004) within this range. In addition, flashes
205 with less than 20 detected sources were not considered in this study (see Section 3 for details).

3 Description of the Charge Layer Polarity Identification Method

207   The charge layer polarity identification method (hereafter Chargepol) consists of an
208 automated algorithm that applies a series of procedures to each lightning flash retrieved by the
209 lmatools, in order to infer charge layer polarity from a flash (link in the Acknowledgments). For
210 reference, Figure 1 shows a flash example with the procedures illustrated. First, flashes with less
211 than 20 sources are disregarded because those flashes would not allow a sufficient number of
212 sources to characterize the initial negative leader breakdown, negative leader propagation
213 through a positive charge region, and sources associated with a negative charge region. Then, all
214 sources contained in the first 10 ms of a flash, referred to here as the Preliminary Breakdown
215 sources (PB sources), are analyzed. A minimum of 4 PB sources is required, and the time
216 interval between the first and last PB source has to be at least 2 ms, in order to better characterize
217 the initial vertical motion of the negative leader. Typical duration periods are between 4 and 10
218 ms for PB (Zheng et al., 2019). We make the assumption that PB sources are associated with
219 negative breakdown having a predominant vertical motion toward a region of positive charge
220 (Shao & Krehbiel, 1996). Hence, linear regression is applied to the PB sources time-height
221 dimension. The linear regression slope is used as a proxy for the vertical speed of the leader, and
222 has to be greater than a threshold of absolute value of 0.05 (0.5 km height variation in 10 ms),
223 which is equivalent to a vertical speed of $5x10^4$ ms^{-1}, or half the typical order of magnitude speed
224 of a negative leader (Behnke et al., 2005; Shao & Krehbiel, 1996; van der Velde & Montanya,
225 2013). By applying that slope threshold, flashes with no clear initial vertical motion are
226 discarded, facilitating further a correct depiction of charge region polarity. In addition, the linear
227 regression fit to the PB sources required a mean squared error (MSE) of less than 0.25 to prevent
228 fitting a regression to noisy sources.

229   Only flashes that satisfy all the aforementioned conditions are used for charge layer
230 depiction, which is typically about 16% of all flashes (more on this in Section 5). The fact that
231 not all flashes are analyzed does not interfere with the objective of this study, because estimating
232 charge polarity for some flashes is sufficient to determine the charge structure evolution over
233 long periods of many hours, as demonstrated in the next section. Next, non-PB sources (sources
234 after 10 ms from flash initiation) are used to infer charge layer polarity, altitude and vertical
235 depth. The PB linear regression intercept altitude is used as a threshold, referred to here as the
236 Charge Height Threshold (CHT), in order to separate positive and negative charge layers
237 candidate sources. For a positive PB linear regression slope (i.e., a flash with initial negative
238 leader moving upward), all non-PB sources above (below) the CHT are candidate sources to
239 define a positive (negative) charge layer. A flash with initial downward motion (negative PB
240 linear regression slope) would have all non-PB sources below (above) the CHT as candidate
241 sources for positive (negative) charge layer. Then, among the candidate sources for each layer
242 polarity, the interval between the 10th and the 90th percentile source heights is used to define a
243 charge layer, which provided a better distinction between positive and negative vertical
244 histograms when compared to other intervals and also neglected sources with possibly doubtful

245 polarity interpretation. For some flashes, it is possible that only one polarity layer is estimated,
246 which leads to the total number of estimated positive layers from flashes for a large period of
247 time being slightly larger than the number of estimated negative layers from flashes.
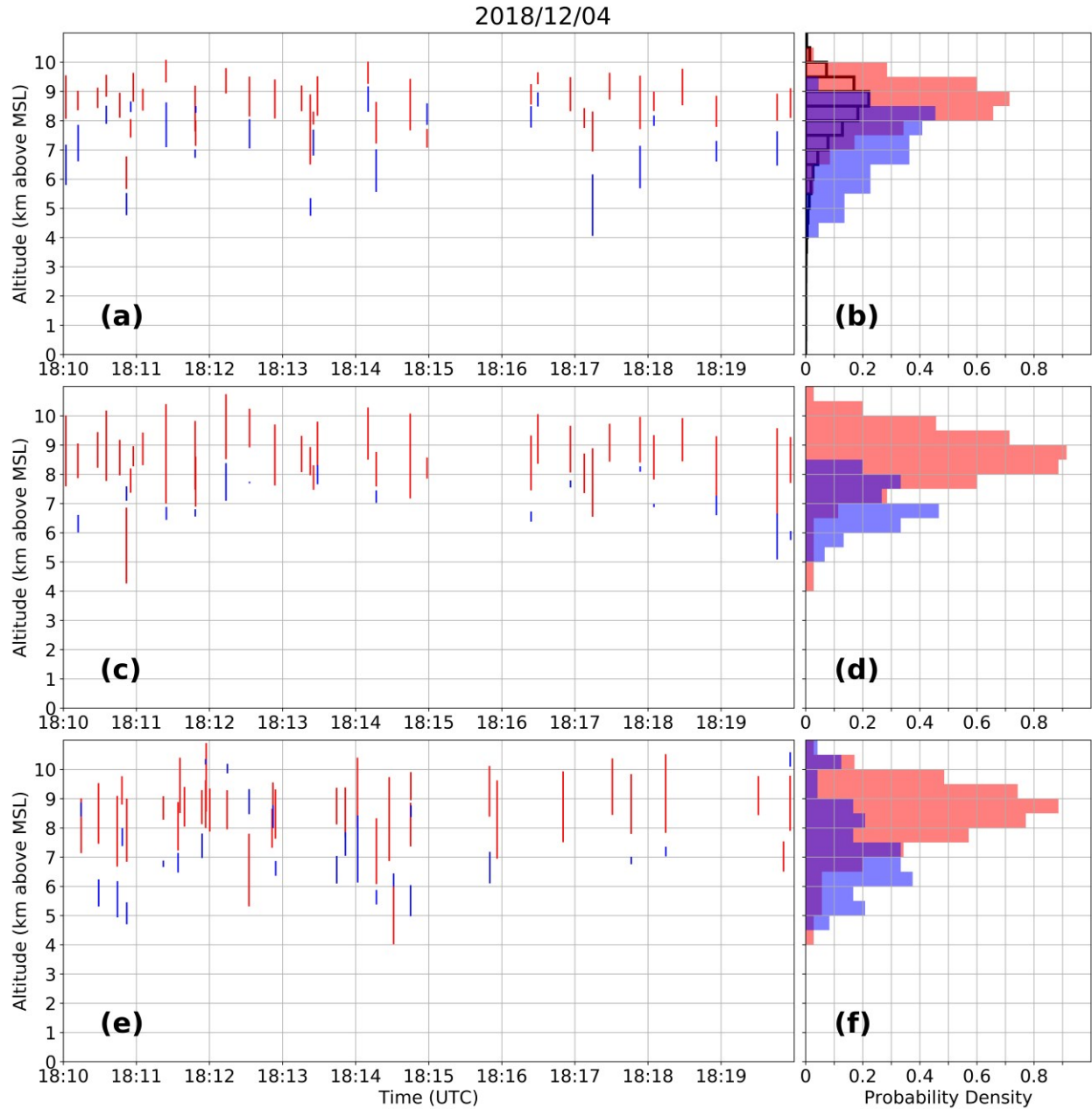

248

249 **Figure 1**. A time-height plot for a positive intracloud flash. The vertical dashed line marks the 10
250 ms time limit that defines the PB sources (black dots). The green line is the linear regression fit
251 on the PB sources. The horizontal dashed line is the CHT (Charge Height Threshold), that
252 separates candidate sources for positive and negative charge layers. Red and blue dots (and
253 shaded areas) define the positive and negative charge layers altitudes and width for this flash,
254 found by applying the interval between the 10th and 90th percentile source altitudes for each
255 polarity candidate sources. Gray dots are candidate sources outside the 10th-90th percentile
256 interval, which were not used to define charge layers.

257 3.1 Validation using Manual Analysis of LMA

258 In order to validate the automated Chargepol identification method, manual polarity
259 inference (Rust et al., 2005; Wiens et al., 2005) was performed on some lightning flashes, and
260 compared with the Chargepol algorithm output. First, a 10-minute period (4 December from
261 1810 to 1820 UTC) with a predominance of normal charge structure (i.e., normal dipole with
262 positive charge over negative charge) was chosen from the RELAMPAGO LMA dataset. Among
263 the 168 flashes that occurred in this period with a normal charge structure, the algorithm
264 estimated charge layers from 35 of them (21%) (Figure 2a). Figures 2b shows a histogram
265 density with the altitude where each charge layer polarity was detected (a peak of positive
266 polarity of 0.7 between 8.5 and 9 km height means that 70% of all positive charge occurred at
267 that level). Source polarities were manually assigned for the same 35 flashes, shown in Figures
268 2c and 2d. The positive charge altitude was estimated to be between about 8 km and 9.5 km from
269 both Chargepol (Figure 2b) and the manual method (Figure 2d). Manual assignment of negative
270 charge (Figure 2d) proved to be challenging, as it could not be estimated from all lightning
271 flashes. Even so, it is notable that the negative charge layer is located at altitudes generally below

272   the altitude of positive charge, with peak occurrence between 6.5 and 7 km height (Figure 2d).
273   Additional validation was performed by assigning polarity for another 35 randomly chosen
274   flashes among the 133 flashes during the same 10-minute period that were not considered by
275   Chargepol (Figure 2e). Most of these flashes did not have a clear vertical trend of the initial
276   leader (not shown). However, as shown in Figure 2f, most positive charge layer detections from
277   flashes were estimated to be between 8 and 9.5 km, consistent with the automated method
278   (Figure 2b), while negative charge is located at lower altitudes. The analysis of an independent
279   subset of flashes from Figures 2e-f demonstrates that Chargepol analysis on a fraction of total
280   flashes is sufficient for the determination of thunderstorm charge structure.
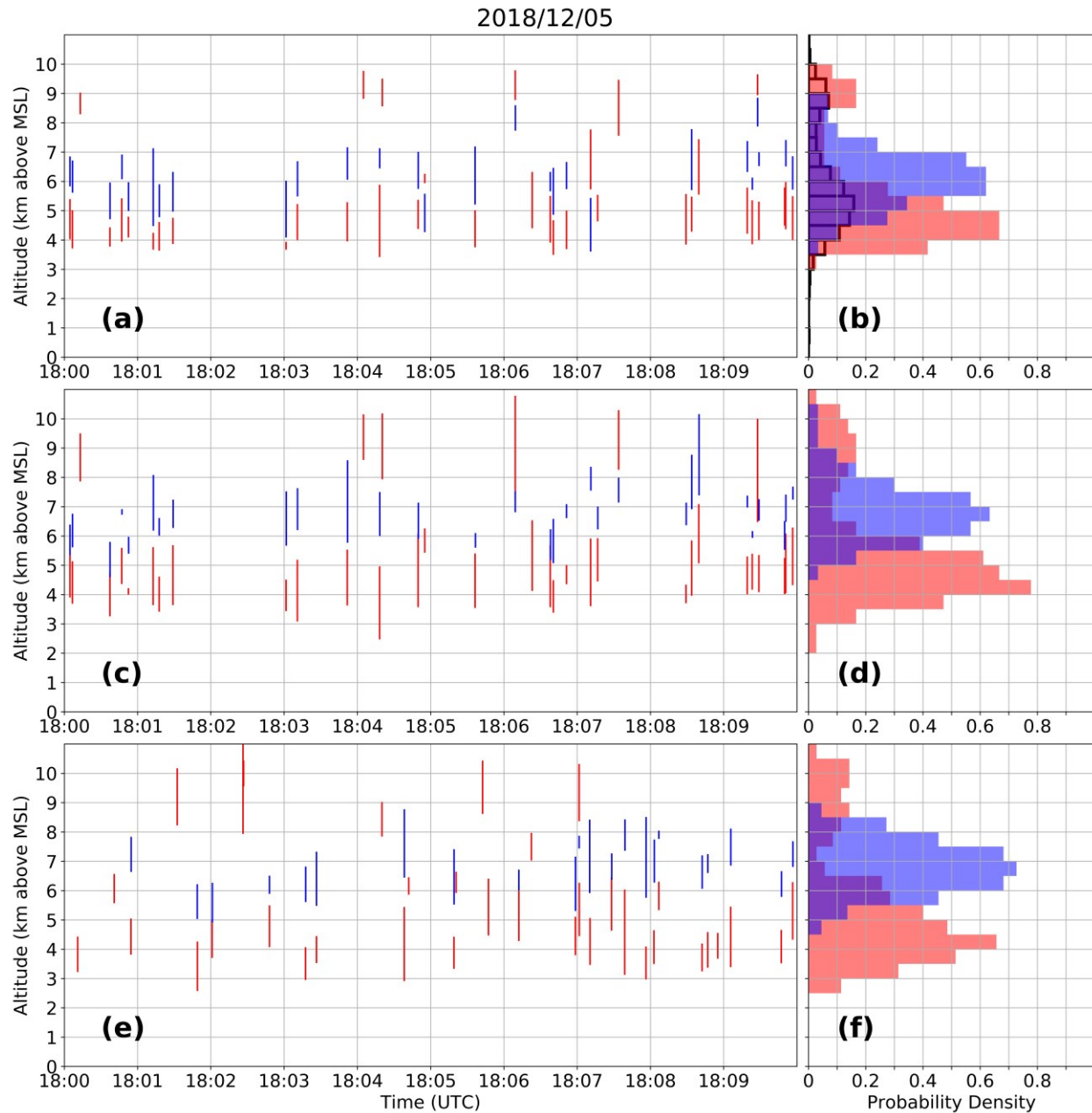

281

282   **Figure 2**. (a) Charge layers estimated from 35 flashes using the Chargepol automated method,
283   (c) polarity assigned manually for the same 35 flashes considered by Chargepol, and (e) polarity

284   assigned manually for 35 other flashes not considered by Chargepol during the same time period.
285   Each red (blue) vertical line represents a positive (negative) charge layer estimated from a flash.
286   (b), (d), and (f) shows histograms (0.5 km bin size) with the probability density of retrieved
287   positive and negative charge layers with height for (a), (c) and (e), respectively (overlap of
288   histograms in purple). Black histogram in (b) shows the source height distribution. The 10-
289   minute period chosen had a predominance of normal charge structure as clearly shown by the
290   Chargepol algorithm, manual analysis, and source distribution.

291   This procedure was repeated for a 10-minute period (5 December from 1800 to 1810
292   UTC) with a predominance of anomalous charge structure (dipole with positive charge located
293   below negative charge), shown in Figure 3. During this period, a high flash rate storm produced
294   mostly negative ICs propagating through a lower positive charge. Another storm with low flash
295   rate and upper positive charge layer was active at the same time. A total of 107 flashes occurred
296   during this period, in which Chargepol estimated charge layers for 36 of them (Figure 3a-b).
297   Manual depiction of charge polarity for these same 36 flashes (Figure 3c) show that the altitudes
298   of positive and negative charge layers (Figure 3d) are in agreement with Chargepol, although
299   manual inference of negative charge is at a slightly higher altitude. From Figure 3d, more than
300   50% of the negative charge layers occurred at altitudes from 6 to 7.5 km, while Chargepol
301   estimated negative charge layers from 5.5 to 7 km height (Figure 3b). The small differences in
302   charge layer altitudes between the manual and automated method demonstrate the small
303   uncertainty of the method. Manual inference for a different set of 36 flashes during the same
304   time period that was not considered by Chargepol is shown in Figures 3e and 3f, and it is
305   consistent with other flashes (Figures 3a and 3c) in locating lower positive charge and mid-level
306   negative charge. The altitude distance between positive and negative charge layers centers (from
307   histogram plots) for all methods is about 2 km. The few upper positive charge layers located
308   above 8.5 km by all methods are from the normal charge structure storm aforementioned.

Figure 3. Same as in Figure 2, but for a 10-minute period with predominance of anomalous charge structure.

The manual depiction of charge layers polarity agrees qualitatively well with the automated depiction. The vertical distance between each polarity's vertical source distribution maxima were sufficiently large by more than 1 km (Fig. 2 and 3 histograms), leading to charge layers being well identified in the vertical dimension.

3.2 Validation using Vertical Distribution of VHF Sources

An additional method to validate the Chargepol algorithm is the estimate of the positive charge layer altitude from the peak in the VHF source histogram (Fuchs et al., 2018; Fuchs &

319   Rutledge 2018; Lang et al., 2020; Lang & Rutledge, 2011). Figures 2b and 3b show an additional
320   histogram of the vertical source density. The histogram for the normal case (Figure 2b) presents
321   the peak at the same altitude the Chargepol method shows a peak with the most occurrences of
322   positive charge. A comparison of these two methods shows that the Chargepol method has the
323   advantage of inferring negative charge layer altitude, which is not possible to estimate from the
324   LMA VHF source distribution. For the anomalous case (Figure 3b), the main low-level peak
325   from the anomalous charge structure storm and the secondary peak from the normal storm are
326   depicted. The peak from the source histogram is at a slightly higher altitude, 5 to 5.5 km,
327   compared to Chargepol's positive inference at 4 to 5 km. However, both methods generally agree
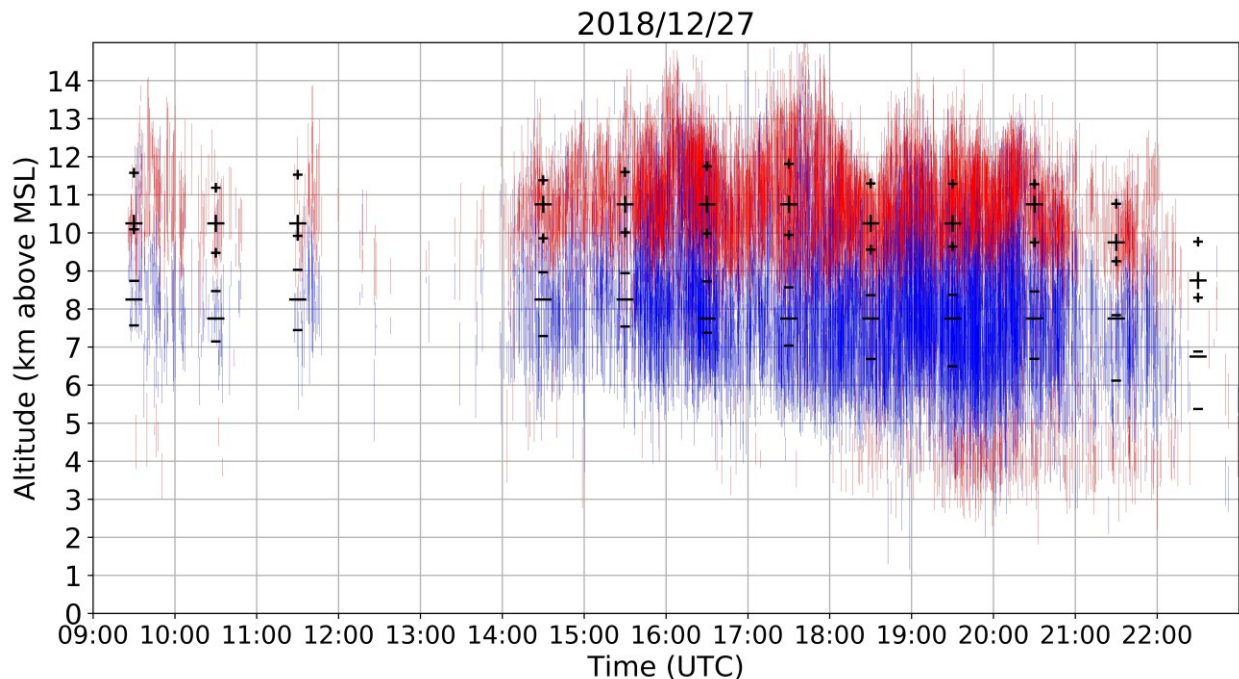328   and the depiction of the negative layer by Chargepol is notable.

329   **4 Chargepol Method Applied to RELAMPAGO Thunderstorms**

330   How charge is structured in Argentinian thunderstorms is generally unknown, and so we
331   make use of the Chargepol method to examine them. During the five-month period the
332   RELAMPAGO LMA network was operating in Cordoba, Argentina. Different storm modes
333   were observed and included isolated convection, multicellular storms, supercells, and mesoscale
334   convective systems (Nesbitt et al. 2021). In order to demonstrate the capability of the algorithm
335   to depict charge structures, examples of distinct Cordoba cases and their evolution in time are
336   presented. Examples of thunderstorms with different charge structures in Cordoba are shown and
337   included normal, anomalous, a case with an enhanced lower positive charge layer, and one that
338   demonstrated a change from one archetype to another through its lifetime. The altitudes at which
339   either positive or negative polarities were classified most frequently, and the mean altitude of
340   tops and bottoms of each charge layer polarity were examined every hour to show how charge
341   layer altitude varied with time for all presented cases. The variation of a dipole's altitude with
342   time depicts a storm's charge structure evolution and it is shown in this study in order to
343   demonstrate a possible application a user can generate with this dataset. For a lower charge layer
344   polarity from a given dipole, the mean altitude of tops and bottoms of charge layers estimated
345   from flashes were only calculated for charge layers in which its top was at a lower altitude than
346   the mean upper dipole polarity altitude. Similarly, for the upper charge layer polarity from a
347   dipole, mean altitude of its top and bottom was obtained from charge layers with its bottom
348   above the altitude of the mean altitude of the lower charge layer polarity. These restrictions were
349   put in place to focus analysis on the top and bottom altitudes of the dominant positive and
350   negative charge layers in the main dipole. To further demonstrate the algorithm's capabilities
351   over regions of the United States that have been studied and well characterized with other charge
352   retrieval methods (e.g., Bruning et al., 2010; MacGorman et al., 2005; Mecikalski et al., 2015;
353   Wiens et al., 2005), an example from each of the LMA networks deployed during DC3 are
354   shown in the supporting information and included a normal tripole case in Alabama, anomalous
355   storms in Colorado, a case with a transition from anomalous to normal charge structure in
356   Oklahoma, and a normal dipole in West Texas at typical altitudes (negative in mid-levels,
357   positive in the upper levels) but with a very high altitude negative charge layer observed above
358   the upper positive.

359   4.1 27 December 2018 Case: Normal Charge Structure

360   Figure 4 shows the estimate of charge layer polarity for all convective storms (most of
361   them multicellular) that occurred in the RELAMPAGO LMA domain for a 14-hour period on 27
362   December 2018. Most thunderstorms that occurred on this day presented an upper-level positive

363 charge layer above 9-10 km height, and a mid-level negative charge layer between about 5 and 9
364 km height. Altitude variation in charge layers is speculated to be due to different thunderstorms
365 having varying updraft strength and cloud-top heights. As the number of charge layers vary
366 within a storm, where more charge layers are found where flash rates are highest (Brothers et al.,
367 2018; DiGangi et al., 2016, for example), we inferred flash rates from periods when charge
368 layers were estimated frequently in short periods of time. For example, more frequently
369 estimated charge layer polarities in shorter timespans were indicative of higher storm flash rates
370 than those less frequently estimated. For most of the period between 1500 and 2100 UTC, the
371 total flash rates of all storms was higher than 50 flashes/minute, considering flashes with more
372 than 10 sources and all active thunderstorms in the domain. The total flash rate of storms in the
373 domain peaked at 195 flashes/minute at 1609 UTC. The dominance of positive over negative
374 charge structure means that most flashes depicted by Chargepol were +ICs, with a typical initial
375 upward motion of a negative leader and further propagation through the upper positive charge
376 layer. This general dipole structure characterizes a typical normal charge structure, as it is
377 common in many regions of the United States as shown in similar LMA-based charge retrieval
378 studies, such as in Alabama (Mecikalski et al., 2015) and Oklahoma (Bruning et al., 2007). Some
379 flashes propagated through a lower positive charge layer below 5 km height, principally after
380 1920 UTC. That was caused by -IC flashes with initial negative leaders with downward motion
381 and further propagation through the low-level positive charge region. Hence, from 1900 to 2200
382 UTC, a typical tripole charge structure (Williams, 1989) was present, though the upper positive
383 region is considerably more active than the lower positive due to more flashes contributing to the
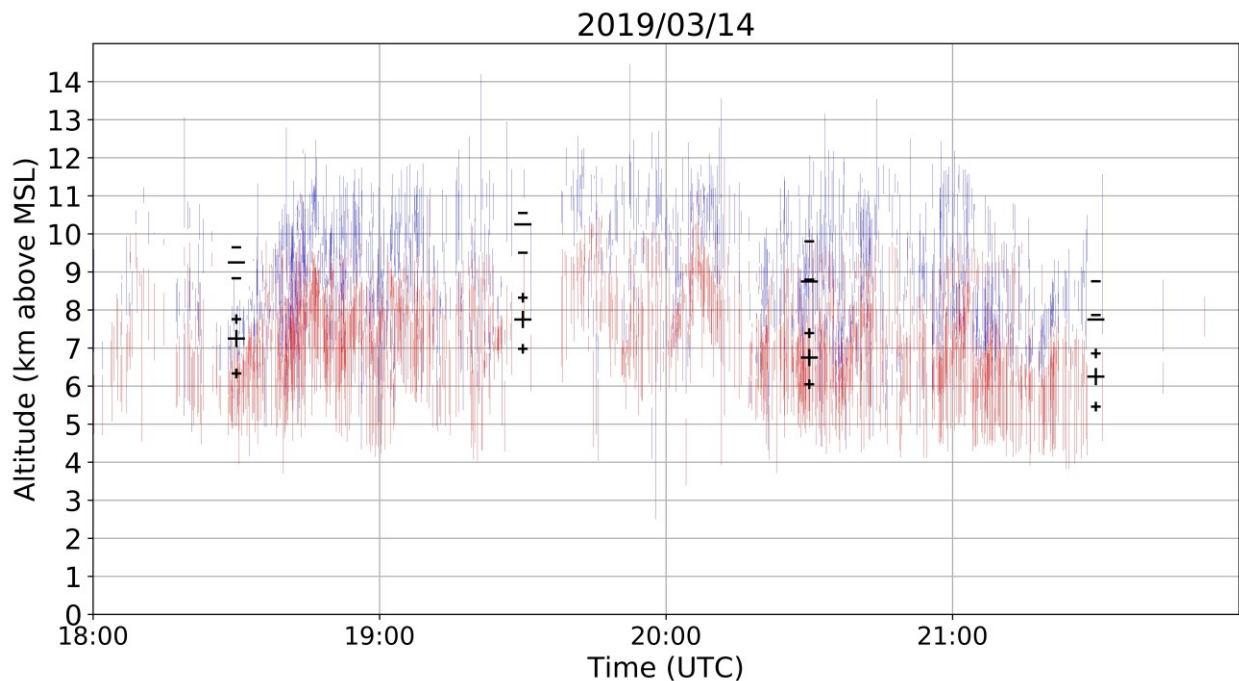384 upper positive depiction.

385

386 **Figure 4**. Charge layers estimated from flashes using the Chargepol automated method for all
387 RELAMPAGO thunderstorms on 27 December 2018 from 0900 to 2300 UTC. Each red (blue)
388 vertical line represents a positive (negative) charge layer estimated from a flash. Large black
389 symbols represent the altitudes in which most charge layers of a certain polarity were estimated
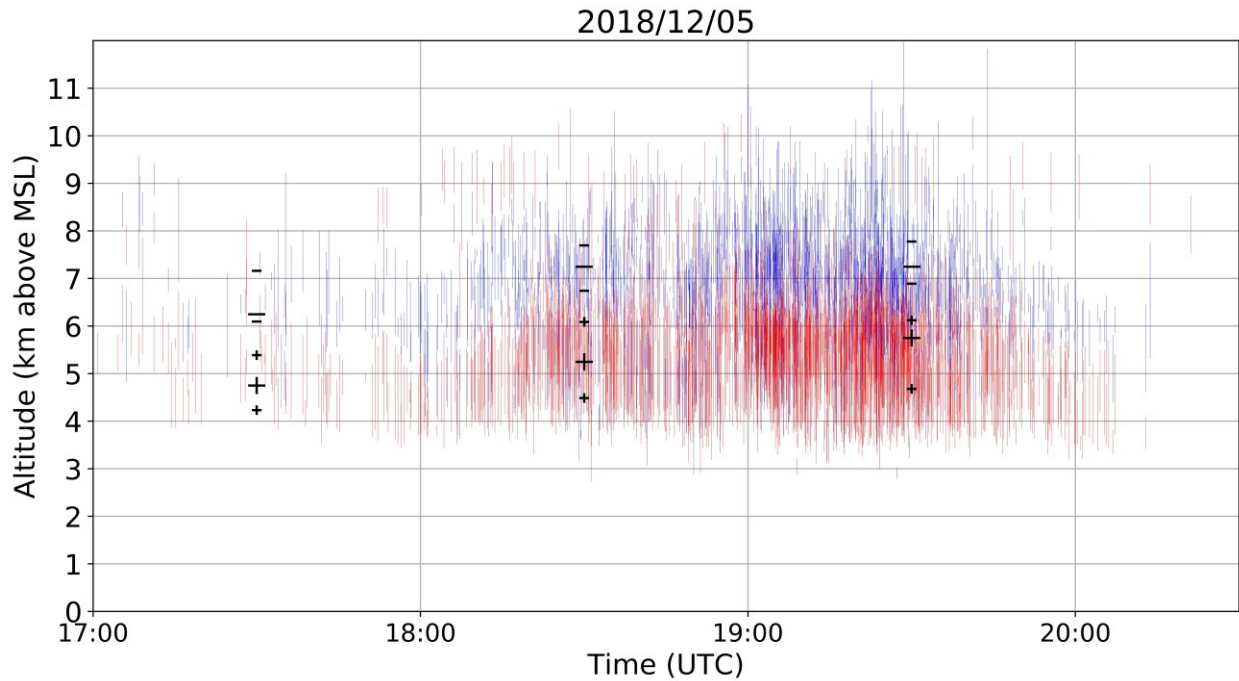
390   for each hour period, as long as more than 30 layers with that polarity were present in that hour.
391   Small black symbols represent the mean altitudes of the top and bottom of charge layers for each
392   polarity and hour.

393   4.2 14 March 2019 and 5 December 2018 Cases: Anomalous Charge Structure

394   A cluster of RELAMPAGO storms on 14 March 2019, all with anomalous dipole charge
395   structures, are shown in Figure 5. These storms had a dominant mid-level positive charge layer
396   and upper-level negative charge layer, similar to some anomalous storms over Colorado (Fuchs
397   et al. 2015). As multiple storms are shown in Figure 5, a large altitude variation is noticeable for
398   the charge layers, which is possibly dependent on individual storm intensity. Storms with
399   stronger updrafts are thought to initiate flashes between charge layers residing at higher altitudes
400   (Stolzenburg et al., 1998). Most flashes in these storms presented -IC lightning, which means
401   that negative breakdown had an initial downward propagation, hence negative charge is
402   estimated at higher levels than positive charge. A similar anomalous dipole case occurred in an
403   isolated thunderstorm on 5 December 2018 (Figure 6). This storm had a flash rate higher than 30
404   flashes/minute for most of the period between 1815 and 1945 UTC, with a peak flash rate of 128
405   flashes/minute at 1902 UTC. This anomalous case is different from the 14 March 2019
406   anomalous case because estimated charge layers are located at lower levels: negative charge is
407   located in the mid-levels, while positive charge is in the low-levels. Also, this was a relatively
408   shallow storm system exhibiting a radar echo top at about 10-km height (not shown), hence no
409   upper positive charge layer had developed. Upper positive charge at about 9 km height from
410   1800 to 1900 UTC was from another storm in the domain (see discussion in Section 3.1).

411

412   **Figure 5**. Same as in figure 4, but for 14 March 2019 from 1800 to 2200 UTC.

413

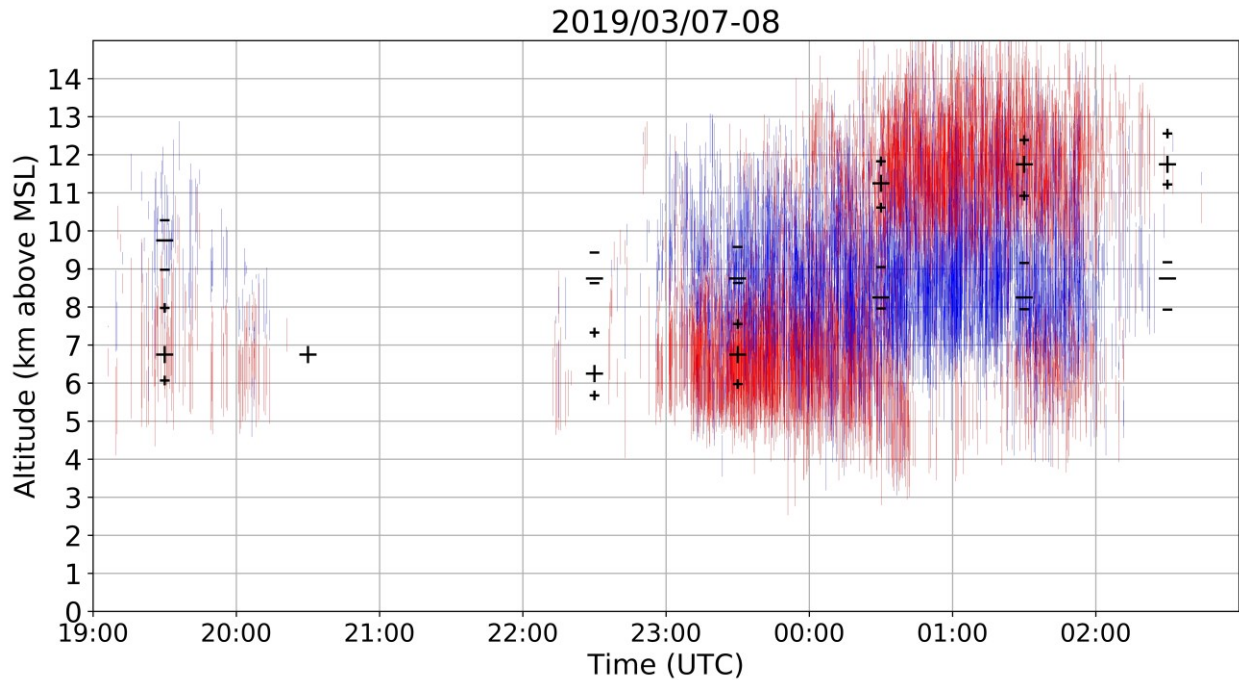414   **Figure 6**. Same as in Figure 4, but for 5 December 2018 from 1700 to 2030 UTC.

415   4.3 7-8 March 2019 Case: Transition from Anomalous to Normal Charge Structure

416   Thunderstorms on 7 March 2019 (Figure 7) during RELAMPAGO presented an
417   anomalous charge structure with mid-level positive charge and upper-level negative charge.
418   From 1900 to 2300 UTC, storms that occurred in the LMA domain had a low flash rate (less than
419   30 flashes/minute considering all thunderstorms in the domain), then few charge layers were
420   depicted by Chargepol, but an anomalous dipole is clearly present, similar to the storm studied
421   by Fuchs et al. (2018) over Colorado. After 2300 UTC, a MCS formed with a dominant
422   anomalous charge structure, with its flash rate rapidly increasing to more than 100 flashes/minute
423   in the LMA domain. On the following UTC day, high flash rates remained, reaching a peak of
424   496 flashes/minute at 0124 UTC in the domain, and an upper positive charge layer formed above
425   10 km height. This upper positive layer became visible because flashes started propagating
426   through that layer. After 0045 UTC, fewer flashes propagated through the lower positive charge
427   layer. Hence, this case characterizes a transition from anomalous to normal charge structure. This
428   case demonstrates how complex charge structure evolution can be estimated by the Chargepol
429   method, such as the presence of anomalous and normal main dipoles, tripoles, and their
430   evolution in time.

Figure 7. Same as in Figure 4, but for 7 March 2019 at 1900 UTC to 8 March 0300 UTC.

5 Frequency of Anomalous Charge Structure in Central Argentina Compared to the U.S.

As the described Chargepol method allows for a relatively fast processing time for large datasets of months of LMA data, one can obtain the general charge structure evolution in time for a domain area, as shown in the previous section. Hence, in order to characterize the likelihood of normal and anomalous charge structure for the five months in which the LMA was deployed in the Cordoba, Argentina region for the first time, the Chargepol layer polarity output was summarized for a better understanding and interpretation of the general dominant charge structure.

In order to achieve a summary of the general charge structure typically occurring in Argentinian storms for long periods of time, the charge polarity information was initially subdivided into time periods of one hour to obtain the dominant dipole for every hour period. Then, the number of charge layers of a given polarity were counted for every altitude in 0.5-km bins for every hour. The altitude with the most positive charge layers estimated from flashes, and the altitude with most negative charge layers, define a single altitude bin for each layer polarity, which characterizes the dominant dipole for that hour, as long as both maximum polarities occur at different heights. A minimum threshold of 30 charge layers from each polarity occurring in one hour was applied, in order to remove the influence of thunderstorms with low flash rates contributing to the charge structure estimation. The large black symbols present in Figures 4-7 represent the altitude with most occurrences of a charge layer polarity for each hour, and the resultant main dominant dipole for an hour period.

In this study, an estimated dipole structure for a one hour period is referred to as a "sample". Samples in which dipoles had positive located at a higher altitude than negative are referred in this study as normal charge structures (Dye et al., 1986; Williams, 1985). A normal charge structure sample could have few flashes that estimated the presence of a low-level

457 positive charge layer, however if more flashes contributed to the maximum height occurrence of
458 positive being at high levels, it would be considered a normal charge structure sample. Figure 4
459 shows an example of a normal tripole charge structure (Williams, 1989) with more positive
460 layers estimated at high levels, leading to a normal dipole estimation. Samples with negative
461 charge over positive charge are considered to have a dominant anomalous charge structure. The
462 most common type of anomalous dipole sample is the type with positive charge at the mid-levels
463 or mixed-phase layer, and negative in the upper levels of a storm (Figure 5). Another structure
464 that could lead to a negative-over-positive dipole is when enhanced positive charge is at low
465 levels of a storm, while negative charge is at the mid-levels (Figure 6, Bruning et al., 2014;
466 Fuchs et al., 2015). In this scenario, an upper positive charge could be present, which could lead
467 to an interpretation of a normal tripole charge structure, an uncommon characteristic during
468 RELAMPAGO as the enhanced low-level positive charge layer is not typically accompanied by
469 an upper-level positive charge layer (Figure 6). However, in this study and others (e.g., Fuchs et
470 al. 2015), a normal tripole scenario with more flashes propagating through the lower positive
471 charge layer than through the upper positive would imply the characterization of an anomalous
472 dipole. Both anomalous scenarios (positive in the mid-levels, and in the low levels) imply that
473 most flashes consisted of -ICs with negative leaders having an initial downward motion, rather
474 than +ICs that would initially move upward. Hence, in this study, scenarios with a dominance of
475 -ICs, or negative-over-positive dipoles, are considered anomalous.
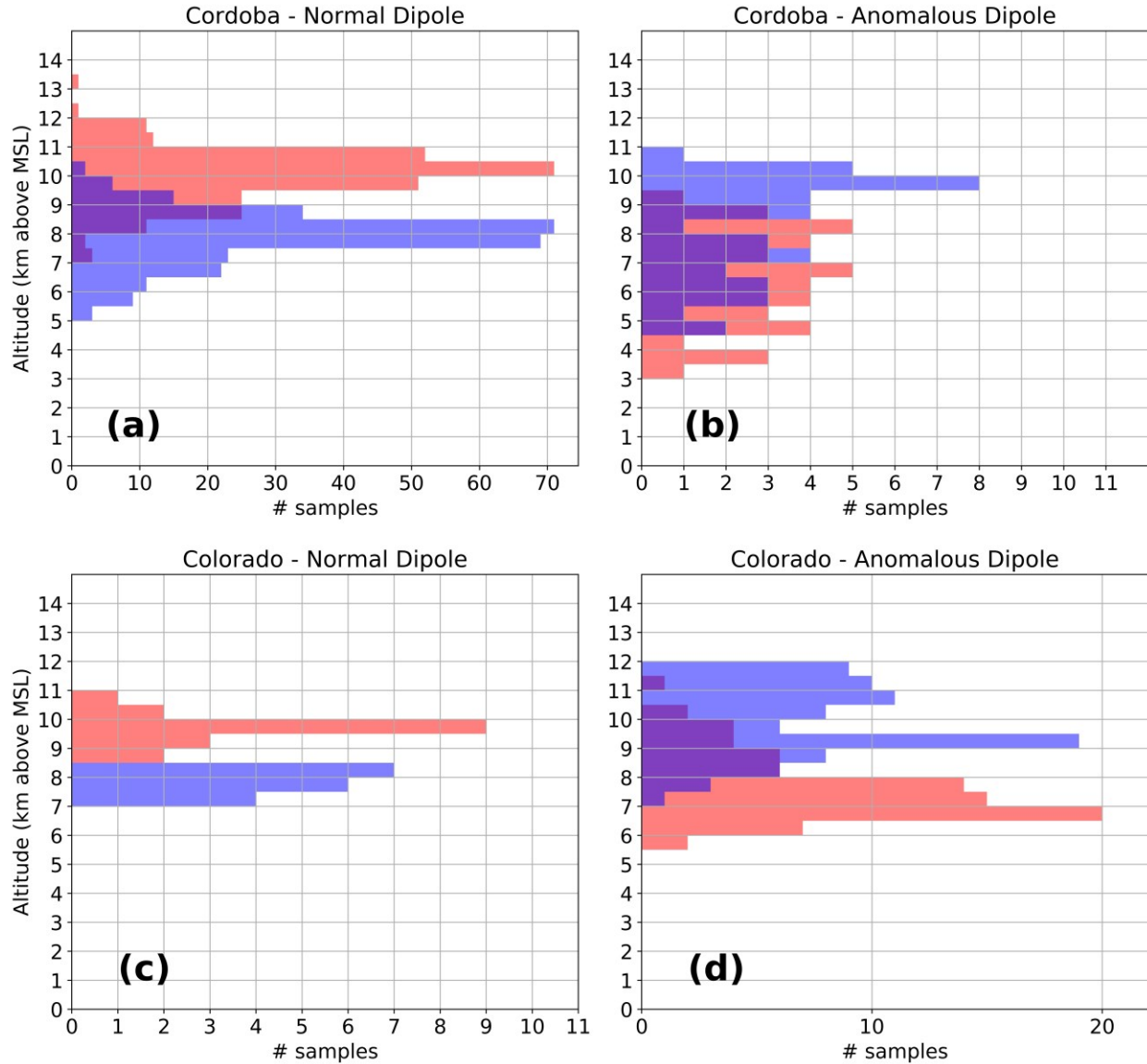
476   During the five months that the LMA was operating in Cordoba, Argentina, 306 samples
477 were observed, which means 306 hours with lightning activity in which the aforementioned
478 methodology estimated a dominant dipole structure. Among the 306 Cordoba samples, 265
479 consisted of normal dipole charge structure, while the other 41 were anomalous (Table 1). That
480 means that 13.3% of samples had a dominant anomalous charge structure, which can be
481 interpreted as an approximate frequency of occurrence of anomalous storms in Cordoba,
482 Argentina. Table 1 shows the number of normal and anomalous samples for the Cordoba LMA
483 deployed during RELAMPAGO, as well as for the four LMA networks deployed during DC3 in
484 several locations across the United States (e.g., Colorado, West Texas, Oklahoma and Alabama)
485 for comparison, all sampled in the warm season (May and June 2012). Table 1 also shows the
486 total number of flashes with more than 20 sources, and the fraction of flashes that were
487 considered by the algorithm, being 16.7% for all LMA networks. The comparison of Cordoba
488 dipole samples with DC3 networks is shown to demonstrate the usefulness of the application and
489 capabilities of Chargepol, as it made estimates of charge structure climatologies similar to those
490 observed in other studies. Even though the sample numbers vary for the different locations,
491 consistent with Carey et al. (2003) and Fuchs and Rutledge (2018), Alabama showed the lowest
492 percentage of anomalous storms (7.3%), and Colorado anomalous frequency was much higher
493 than any other region (82.6%). Oklahoma and West Texas fell in between these two regions, and
494 with similar anomalous frequencies to Cordoba (12.9% for Oklahoma and 11.1% for West
495 Texas). From the flash centroid altitude distribution for the entire RELAMPAGO LMA dataset,
496 Lang et al. (2020), observed a peak at 10 km height and a secondary peak at 6 km height, the
497 latter attributed to anomalous storms and stratiform lightning. For the normal and anomalous
498 Cordoba events shown in Lang et al. (2020), normal and anomalous samples were consistently
499 depicted by the Chargepol algorithm.

500   **Table 1.** Number of normal and anomalous samples for Cordoba, Alabama, West Texas,
501   Oklahoma, and Colorado.

	Cordoba	Alabama	West Texas	Oklahoma	Colorado
Number of days	157	32	48	41	61
Number of flashes (>20 sources)	808416	39046	261713	497139	545005
Number of flashes considered by Chargepol	165767 (20.5%)	7653 (19.5%)	65309 (24.9%)	58900 (11.8%)	62556 (11.4%)
Total number of samples	306	41	99	80	98
Normal samples	265	38	88	70	17
Anomalous samples	41	3	11	10	81
% Anomalous	13.3	7.3	11.1	12.5	82.6

502   The distribution of normal samples with altitude demonstrated that most normal dipoles
503   were present in the mid-to-upper levels; i.e., with mid-level negative and upper-level positive
504   charge. Figure 8a shows the distribution of normal dipoles for Cordoba, Argentina. The altitude
505   distribution of anomalous samples (i.e., negative over positive dipoles) in Argentina shows that
506   there were cases in which negative charge was present in the upper levels with positive in the
507   mid-levels, and cases of negative in the mid-levels, with enhanced positive in the low levels
508   (Figure 8b). In Colorado, few normal samples were observed, but their altitude distribution is
509   similar to Cordoba (Figure 8c). The distribution of anomalous samples with altitude in Colorado
510   showed that most dipoles had upper level negative and mid-level positive. No apparent presence
511   of an anomalous dipole located in the low-mid-levels occurred in the Colorado DC3 LMA
512   dataset. Therefore, the Cordoba 5 December 2018 case (Figure 6) demonstrates a singular
513   thunderstorm charge structure that is either rare or completely absent in Colorado. The normal
514   sample distributions in height for the other 3 U.S. locations (not shown) were similar to Cordoba
515   and Colorado, while the anomalous sample distribution for these 3 locations (not shown) proved
516   inconclusive due to the low sample number.

Figure 8. Distribution of normal and anomalous samples with altitude for Cordoba (a, b) and Colorado (c, d).

6 Summary and Discussion

This paper presented charge structures for the warm season thunderstorms in Cordoba, Argentina for the first time through thunderstorm examples and long-term statistics utilizing a new method that identifies charge layer polarity at a flash level from LMA VHF data. This method is able to estimate general charge structures such as normal and anomalous dipoles, tripoles, altitude and vertical depth of charge layers. Chargepol was applied to months of LMA data, allowing for the inference of the frequency of anomalous and normal charge structure thunderstorms in Cordoba, Argentina, and comparison to four well-studied U.S. regions using the same methodology.

529   This method was developed from a meteorological standpoint, which means that the
530   objective was to obtain the general charge structure evolution through the entire thunderstorm
531   life cycle, or for many hours of data. In order to achieve that, there was no need to retrieve
532   charge polarity from every flash as demonstrated in the comparison of Chargepol relative to
533   manual charge structure analysis and the VHF source distribution peak. Instead, only flashes
534   with less doubtful characteristics were used to provide an accurate charge polarity retrieval.
535   Hence, when considering such long periods of time, the frequency of anomalous and normal
536   charge structures can be estimated. Also, we found that it is sufficient to summarize the data into
537   the main dominant dipoles for every hour in order to characterize the charge structure for a
538   region. It is important to emphasize that, once charge layers are retrieved from individual
539   lightning flashes, one can organize this same dataset in any other manner depending on the user's
540   purpose. Examples include considering the algorithm output as a database to be organized into
541   shorter or longer time periods, obtaining the density of charge layers polarity over the time-
542   altitude domain, calculating statistics for comparison with observations from other
543   instrumentation such as radar, etc.

544   The complexities of a three-dimensional charge structure that may be present at sub-
545   storm scale, with charge layers extending through different altitudes depending on distance to an
546   updraft core, are not being fully accounted for in this study. For a flash analysis, we consider the
547   charge distribution over the vertical dimension only, which proved to be sufficient for this
548   study's objectives. For a given flash, the Chargepol method can estimate no more than two
549   charge layers with opposite polarities. However, when observing charge layers output for
550   numerous flashes, it is possible to infer the presence of dipoles, their altitude and time evolution,
551   the presence of tripoles and even multiple charge layers if flashes propagate through it. Only
552   charge layers that had flashes moving through them can be inferred. In the case of a positive
553   charge layer without a lightning flash moving through it, the charge layer cannot be visualized as
554   a product of the algorithm, which is a fundamental limitation of all LMA-based charge retrieval
555   methods (Rust et al., 2005). The fact that Chargepol neglects small flashes for charge layer
556   estimation, as it discards flashes with less than 20 sources, makes it hard to locate small pockets
557   of charge within thunderstorms. Even if these charge regions were located, it could be hard to
558   visualize and interpret their evolution over minutes. Also, differentiating charge structure of
559   small flashes from noise would be challenging, an issue to be addressed in a future study. In
560   order for small flashes to be included in the analysis for identification of finer charge structures,
561   threshold of parameters have to be relaxed prior to running Chargepol. However, estimating the
562   general dipole and tripole charge structures is feasible with the conditions used in this study,
563   satisfying our purpose.

564   The Chargepol method proved capable for analyzing large LMA datasets in a reasonable
565   processing time of minutes, allowing for efficient interpretation of charge structures over
566   Cordoba, Argentina during the recent RELAMPAGO field campaign and a consistent
567   comparison of these novel results with thunderstorms from different regions of the United States
568   whose charge structures have been sampled with LMA and are more well understood. A high
569   frequency of anomalous storms were found for Colorado consistent with other studies (Fuchs et
570   al., 2018). Examples of Cordoba anomalous thunderstorms with altitude distributions of positive
571   charge layers that are uncommon in Colorado were presented. Interestingly, Cordoba showed
572   slightly higher anomalous charge structure frequency compared to Oklahoma and West Texas,
573   while Alabama presented the lowest anomalous frequency among all studied regions consistent
574   with prior work (Fuchs et al., 2018). Reasonings for these results were not explored in this study.

575 The meteorological, environmental, kinematic and microphysical conditions in Central
576 Argentina are speculated to be important contributors to the observed charge structures
577 documented herein during RELAMPAGO, and they will be explored in future studies and
578 compared to past work from other regions throughout the world. The charge polarity outputs
579 presented in this study have the potential to be useful for numerous applications in lightning
580 research, and Chargepol has been made available as an open-source algorithm with options to
581 choose parameter thresholds.

Acknowledgments and Data

References

593 Baker, B., Baker, M. B., Jayaratne, E. R., Latham, J., & Saunders, C. P. R. (1987). The influence
594 of diffusional growth rates on the charge transfer accompanying rebounding collisions between
595 ice crystals and soft hailstones. *Quarterly Journal of the Royal Meteorological Society,*
596 *113*(478), 1193-1215. https://doi.org/10.1002/qj.49711347807

597 Baker, B., Baker, M. B., Jayaratne, E. R., Latham, J., & Saunders, C. P. R. (1987). The influence
598 of diffusional growth rates on the charge transfer accompanying rebounding collisions between
599 ice crystals and soft hailstones. *Quarterly Journal of the Royal Meteorological Society,*
600 *113*(478), 1193-1215. https://doi.org/10.1002/qj.49711347807

601 Barth, M. C., Cantrell, C. A., Brune, W. H., Rutledge, S. A., Crawford, J. H., Huntrieser, H., et
602 al. (2015). The deep convective clouds and chemistry (DC3) field campaign. *Bulletin of the*
603 *American Meteorological Society, 96*(8), 1281-1309. https://doi.org/10.1175/BAMS-D-13-
604 00290.1

605 Behnke, S. A., Thomas, R. J., Krehbiel, P. R. & Rison, W. (2005). Initial leader velocities during
606 intracloud lightning: Possible evidence for a runaway breakdown effect. *Journal of Geophysical*
607 *Research: Atmospheres*, *110*(D10). https://doi.org/10.1029/2004JD005312

608 Berdeklis, P. & List, R. (2001). The ice crystal–graupel collision charging mechanism of
609 thunderstorm electrification. *Journal of the Atmospheric Sciences, 58*(18), 2751-2770.
610 https://doi.org/10.1175/1520-0469(2001)058<2751:TICGCC>2.0.CO;2

611 Brooks, I. M., Saunders, C. P. R., Mitzeva, R. P., & Peck, S. L. (1997). The effect on
612 thunderstorm charging of the rate of rime accretion by graupel. *Atmospheric Research, 43*(3),
613 277-295. https://doi.org/10.1016/S0169-8095(96)00043-9

Brothers, M. D., Bruning, E. C., & Mansell, E. R. (2018). Investigating the relative contributions of charge deposition and turbulence in organizing charge within a thunderstorm. *Journal of the Atmospheric Sciences*, *75*(9), 3265-3284. https://doi.org/10.1175/JAS-D-18-0007.1

Bruning E. C., Rust, W. D., Schuur, T. J., MacGorman, D. R., Krehbiel, P. R., & Rison, W. (2007). Electrical and polarimetric radar observations of a multicell storm in TELEX. *Monthly Weather Review, 135*(7), 2525-2544. https://doi.org/10.1175/MWR3421.1

Bruning E. C., Rust, W. D., MacGorman, D. R., Biggerstaff, M. I., & Schuur, T. J. (2010). Formation of charge structures in a supercell. *Monthly Weather Review, 138*(10), 3740-3761. https://doi.org/10.1175/2010MWR3160.1

Bruning E. C., Weiss, S. A., & Calhoun, K. M. (2014). Continuous variability in thunderstorm primary electrification and an evaluation of inverted-polarity terminology. *Atmospheric research, 135*, 274-284. https://doi.org/10.1016/j.atmosres.2012.10.009

Bruning E. C. (2015). lmatools: Python code for working with VHF Lightning Mapping Array data. https://doi.org/10.5281/zenodo.32510

Calhoun, K. M., MacGorman, D. R., Ziegler, C. L., & Biggerstaff, M. I. (2013). Evolution of lightning activity and storm charge relative to dual-Doppler analysis of a high-precipitation supercell storm. *Monthly Weather Review, 141*(7), 2199-2223. https://doi.org/10.1175/MWR-D-12-00258.1

Carey, L. D., Rutledge, S. A., & Petersen, W. A. (2003). The relationship between severe storm reports and cloud-to-ground lightning polarity in the contiguous United States from 1989 to 1998. *Monthly Weather Review, 131*(7), 1211-1228. https://doi.org/10.1175/1520-0493(2003)131<1211:TRBSSR>2.0.CO;2

Cecil, D. J. & Blankenship, C. B. (2012). Toward a global climatology of severe hailstorms as estimated by satellite passive microwave imagers. *Journal of Climate, 25*(2), 687-703. https://doi.org/10.1175/JCLI-D-11-00130.1

Chmielewski, V. C., & Bruning, E. C. (2016). Lightning Mapping Array flash detection performance with variable receiver thresholds. *Journal of Geophysical Research: Atmospheres*, *121*(14), 8600-8614. https://doi.org/10.1002/2016JD025159

Chmielewski, V. C., Bruning, E. C., & Ancell, B. C. (2018). Variations of Thunderstorm Charge Structures in West Texas on 4 June 2012. *Journal of Geophysical Research: Atmospheres, 123*(17), 9502-9523. https://doi.org/10.1029/2018JD029006

Coleman, L. M., Marshall, T. C., Stolzenburg, M., Hamlin, T., Krehbiel, P. R., Rison, W. & Thomas, R. J. (2003). Effects of charge and electrostatic potential on lightning propagation. *Journal of Geophysical Research: Atmospheres*, *108*(D9). https://doi.org/10.1029/2002JD002718

649 DiGangi, E. A., MacGorman, D. R., Ziegler, C. L., Betten, D., Biggerstaff, M., Bowlan, M., &
650 Potvin, C. K. (2016). An overview of the 29 May 2012 Kingfisher supercell during DC3. *Journal*
651 *of Geophysical Research: Atmospheres, 121*(24). https://doi.org/10.1002/2016JD025690

652 Dye, J. E., Jones, J. J., Winn, W. P., Cerni, T. A., Gardiner, B., Lamb, D., et al. (1986). Early
653 electrification and precipitation development in a small, isolated Montana cumulonimbus.
654 *Journal of Geophysical Research: Atmospheres, 91*(D1), 1231-1247.
655 https://doi.org/10.1029/JD091iD01p01231

656 Dye, J. E., Jones, J. J., Weinheimer, A. J., & Winn, W. P. (1988). Observations within two
657 regions of charge during initial thunderstorm electrification. *Quarterly Journal of the Royal*
658 *Meteorological Society, 114*(483), 1271-1290. https://doi.org/10.1002/qj.49711448306

659 Dye, J. E., Winn, W. P., Jones, J. J., & Breed, D. W. (1989). The electrification of New Mexico
660 thunderstorms: 1. Relationship between precipitation development and the onset of
661 electrification. *Journal of Geophysical Research: Atmospheres, 94*(D6), 8643-8656.
662 https://doi.org/10.1029/JD094iD06p08643

663 Emersic, C., Heinselman, P. L., MacGorman, D. R., & Bruning, E. C. (2011). Lightning activity
664 in a hail-producing storm observed with phased-array radar. *Monthly Weather Review, 139*(6),
665 1809-1825. https://doi.org/10.1175/2010MWR3574.1

666 Emersic, C. & Saunders, C. P. R. (2010). Further laboratory investigations into the relative
667 diffusional growth rate theory of thunderstorm electrification. *Atmospheric Research*, *98*(2-4),
668 327-340. https://doi.org/10.1016/j.atmosres.2010.07.011

669 Ester, M., Kriegel, H. P., Sander, J., & Xu, X. (1996). A density-based algorithm for discovering
670 clusters in large spatial databases with noise. In *Kdd, 96*(34), 226-231.

671 Fuchs, B. R., Rutledge, S. A., Bruning, E. C., Pierce, J. R., Kodros, J. K., Lang, T. J., et al.
672 (2015). Environmental controls on storm intensity and charge structure in multiple regions of the
673 continental United States. *Journal of Geophysical Research: Atmospheres, 120*(13), 6575-6596.
674 https://doi.org/10.1002/2015JD023271

675 Fuchs, B. R., Bruning, E. C., Rutledge, S. A., Carey, L. D., Krehbiel, P. R., & Rison, W. (2016).
676 Climatological analyses of LMA data with an open-source lightning flash-clustering algorithm.
677 *Journal of Geophysical Research: Atmospheres, 121*(14), 8625-8648.
678 https://doi.org/10.1002/2015JD024663

679 Fuchs, B. R. & Rutledge, S. A. (2018). Investigation of lightning flash locations in isolated
680 convection using LMA observations. *Journal of Geophysical Research: Atmospheres, 123*(11),
681 6158-6174. https://doi.org/10.1002/2017JD027569

682 Fuchs, B. R., Rutledge, S. A., Dolan, B., Carey, L. D., & Schultz, C. (2018). Microphysical and
683 kinematic processes associated with anomalous charge structures in isolated convection. *Journal*
684 *of Geophysical Research: Atmospheres, 123*, 6505-6528. https://doi.org/10.1029/2017JD027540

685 Goodman, S. J., Blakeslee, R., Christian, H., Koshak, W., Bailey, J., Hall, J., et al. (2005). The
686 North Alabama lightning mapping array: Recent severe storm observations and future prospects.
687 *Atmospheric Research, 76*(1-4), 423-437. https://doi.org/10.1016/j.atmosres.2004.11.035

688 Kasemir, H. W. (1960). A contribution to the electrostatic theory of a lightning discharge.
689 *Journal of Geophysical Research, 65*(7), 1873-1878. https://doi.org/10.1029/JZ065i007p01873

690 Krehbiel, P. R., Thomas, R. J., Rison, W., Hamlin, T., Harlin, J., & Davis, M. (2000). GPS-based
691 mapping system reveals lightning inside storms. *Eos, Transactions American Geophysical
692 Union, 81*(3), 21-25. https://doi.org/10.1029/00EO00014

693 Koshak, W. J. & Solakiewicz, R. J. (1996). On the retrieval of lightning radio sources from time-
694 of-arrival data. *Journal of Geophysical Research: Atmospheres, 101*(D21), 26631-26639.
695 https://doi.org/10.1029/96JD01618

696 Koshak, W. J., Solakiewicz, R. J., Blakeslee, R. J., Goodman, S. J., Christian, H. J., Hall, J. M.,
697 et al. (2004). North Alabama Lightning Mapping Array (LMA): VHF source retrieval algorithm
698 and error analyses. *Journal of Atmospheric and Oceanic Technology, 21*(4), 543-558.
699 https://doi.org/10.1175/1520-0426(2004)021<0543:NALMAL>2.0.CO;2

700 Lang, T. J., & Rutledge, S. A. (2002). Relationships between convective storm kinematics,
701 precipitation, and lightning. *Monthly Weather Review, 130*(10), 2492-2506.
702 https://doi.org/10.1175/1520-0493(2002)130<2492:RBCSKP>2.0.CO;2

703 Lang, T. J., & Rutledge, S. A. (2008). Kinematic, microphysical, and electrical aspects of an
704 asymmetric bow-echo mesoscale convective system observed during STEPS 2000. *Journal of
705 Geophysical Research*, *113*(D08213). https://doi.org/10.1029/2006JD007709

706 Lang, T. J., & Rutledge, S. A. (2011). A framework for the statistical analysis of large radar and
707 lightning datasets: Results from STEPS 2000. *Monthly Weather Review, 139*(8), 2536-2551.
708 https://doi.org/10.1175/MWR-D-10-05000.1

709 Lang, T. J., Ávila, E. E., Blakeslee, R. J., Burchfield, J., Wingo, M., Bitzer, P. M., et al. (2020).
710 The RELAMPAGO Lightning Mapping Array: Overview and initial comparison to the
711 Geostationary Lightning Mapper. *Journal of Atmospheric and Oceanic Technology, 37*(8), 1457-
712 1475. https://doi.org/10.1175/JTECH-D-20-0005.1

713 Lhermitte, R. & Krehbiel, P. R. (1979). Doppler radar and radio observations of thunderstorms.
714 *IEEE Transactions on Geoscience Electronics, 17*(4), 162-171.
715 https://doi.org/10.1109/TGE.1979.294644

716 López, J. A., Montanyà, J., van der Velde, O. A., Pineda, N., Salvador, A., Romero, D., et al.
717 (2019). Charge structure of two tropical thunderstorms in Colombia. *Journal of Geophysical
718 Research: Atmospheres, 124*(10), 5503-5515. https://doi.org/10.1029/2018JD029188

719 Lund, N. R., MacGorman, D. R., Schuur, T. J., Biggerstaff, M. I., & Rust, W. D. (2009).
720 Relationships between lightning location and polarimetric radar signatures in a small mesoscale

721   convective system. *Monthly Weather Review, 137*(12), 4151-4170.
722   https://doi.org/10.1175/2009MWR2860.1

723   MacGorman, D. R., Rust, W. D., Krehbiel, P., Rison, W., Bruning, E., & Wiens, K. (2005). The
724   electrical structure of two supercell storms during STEPS. *Monthly Weather Review, 133*(9),
725   2583-2607. https://doi.org/10.1175/MWR2994.1

726   MacGorman, D. R., Rust, W. D., Schuur, T. J., Biggerstaff, M. I., Straka, J. M., Ziegler, C. L., et
727   al. (2008). TELEX the thunderstorm electrification and lightning experiment. *Bulletin of the
728   American Meteorological Society, 89*(7), 997-1014. https://doi.org/10.1175/2007BAMS2352.1

729   Marshall, T. C., Rust, W. D., & Stolzenburg, M. (1995). Electrical structure and updraft speeds
730   in thunderstorms over the southern Great Plains. *Journal of Geophysical Research: Atmospheres,
731   100*(D1), 1001-1015. https://doi.org/10.1029/94JD02607

732   Mazur, V. & Ruhnke, L. H. (1993). Common physical processes in natural and artificially
733   triggered lightning. *Journal of Geophysical Research: Atmospheres, 98*(D7), 12913-12930.
734   https://doi.org/10.1029/93JD00626

735   Mecikalski, R. M., Bain, A. L., & Carey, L. D. (2015). Radar and lightning observations of deep
736   moist convection across northern Alabama during DC3: 21 May 2012. *Monthly Weather
737   Review, 143*(7), 2774-2794. https://doi.org/10.1175/MWR-D-14-00250.1

738   Nesbitt, S. W., Salio, P. V., Avila, E., Bitzer, P., Carey, L., Chandrasekar, V., et al. (2021). A
739   storm safari in Subtropical South America: Proyecto RELAMPAGO. *Bulletin of the American
740   Meteorological Society.* 1-64. https://doi.org/10.1175/BAMS-D-20-0029.1

741   Orville, R. E. & Huffines, G. R. (2001). Cloud-to-ground lightning in the United States: NLDN
742   results in the first decade, 1989–98. *Monthly Weather Review*, *129*(5), 1179-1193.
743   https://doi.org/10.1175/1520-0493(2001)129<1179:CTGLIT>2.0.CO;2

744   Pawar, S. D., & Kamra, A. K. (2004). Evolution of lightning and the possible
745   initiation/triggering of lightning discharges by the lower positive charge center in an isolated
746   thundercloud in the tropics. *Journal of Geophysical Research: Atmospheres, 109*(D2).
747   https://doi.org/10.1029/2003JD003735

748   Pereyra, R. G., Avila, E. E., Castellano, N. E., & Saunders, C. P. (2000). A laboratory study of
749   graupel charging. *Journal of Geophysical Research: Atmospheres, 105*(D16), 20803-20812.
750   https://doi.org/10.1029/2000JD900244

751   Pineda, N., Rigo, T., Montanyà, J., & van der Velde, O. A. (2016). Charge structure analysis of a
752   severe hailstorm with predominantly positive cloud-to-ground lightning. *Atmospheric Research,
753   178*, 31-44. https://doi.org/10.1016/j.atmosres.2016.03.010

754   Qie, X., Zhang, T., Chen, C., Zhang, G., Zhang, T., & Wei, W. (2005). The lower positive
755   charge center and its effect on lightning discharges on the Tibetan Plateau. *Geophysical
756   Research Letters*, *32*(L05814). https://doi.org/10.1029/2004GL022162

757 Rasmussen, K. L., Zuluaga, M. D., & Houze Jr, R. A. (2014). Severe convection and lightning in
758 subtropical South America. *Geophysical Research Letters, 41*(20), 7359-7366.
759 https://doi.org/10.1002/2014GL061767

760 Rison, W., Thomas, R. J., Krehbiel, P. R., Hamlin, T., & Harlin, J. (1999). A GPS-based three-
761 dimensional lightning mapping system: Initial observations in central New Mexico. *Geophysical*
762 *Research Letters, 26*(23), 3573-3576. https://doi.org/10.1029/1999GL010856

763 Rust, W. D. & MacGorman, D. R. (2002). Possibly inverted-polarity electrical structures in
764 thunderstorms during STEPS. *Geophysical Research Letters, 29*(12), 12-1.
765 https://doi.org/10.1029/2001GL014303

766 Rust, W. D., MacGorman, D. R., Bruning, E. C., Weiss, S. A., Krehbiel, P. R., Thomas, R. J., et
767 al. (2005). Inverted-polarity electrical structures in thunderstorms in the Severe Thunderstorm
768 Electrification and Precipitation Study (STEPS). *Atmospheric Research, 76*(1-4), 247-271.
769 https://doi.org/10.1016/j.atmosres.2004.11.029

770 Saunders, C. P. R., Keith, K. W., & Mitzeva, R. P. (1991). The effect of liquid water on
771 thunderstorm charging. *Journal of Geophysical Research: Atmospheres, 96*(D6), 11007-11017.
772 https://doi.org/10.1029/91JD00970

773 Saunders, C. P. R. & Peck, S. L. (1998). Laboratory studies of the influence of the rime accretion
774 rate on charge transfer during crystal/graupel collisions. *Journal of Geophysical Research:*
775 *Atmospheres, 103*(D12), 13949-13956. https://doi.org/10.1029/97JD02644

776 Saunders, C. P. R., Peck, S. L., Varela, G. A., Avila, E. E., & Castellano, N. E. (2001). A
777 laboratory study of the influence of water vapour and mixing on the charge transfer process
778 during collisions between ice crystals and graupel. *Atmospheric Research, 58*(3), 187-203.
779 https://doi.org/10.1016/S0169-8095(01)00090-4

780 Saunders, C. P. R., Bax-Norman, H., Emersic, C., Avila, E. E., & Castellano, N. E. (2006).
781 Laboratory studies of the effect of cloud conditions on graupel/crystal charge transfer in
782 thunderstorm electrification. *Quarterly Journal of the Royal Meteorological Society: A journal of*
783 *the atmospheric sciences, applied meteorology and physical oceanography, 132*(621), 2653-
784 2673. https://doi.org/10.1256/qj.05.218

785 Shao, X. M. & Krehbiel, P. R. (1996). The spatial and temporal development of intracloud
786 lightning. *Journal of Geophysical Research: Atmospheres, 101*(D21), 26641-26668.
787 https://doi.org/10.1029/96JD01803

788 Stolzenburg, M., Rust, W. D., Smull, B. F., & Marshall, T. C. (1998). Electrical structure in
789 thunderstorm convective regions: 1. Mesoscale convective systems. *Journal of Geophysical*
790 *Research: Atmospheres, 103*(D12), 14059-14078. https://doi.org/10.1029/97JD03546

791 Stough, S. M. & Carey, L. D. (2020). Observations of Anomalous Charge Structures in Supercell
792 Thunderstorms in the Southeastern United States. *Journal of Geophysical Research:*
793 *Atmospheres, 125*(17), p.e2020JD033012. https://doi.org/10.1029/2020JD033012

794   Takahashi, T. (1978). Riming electrification as a charge generation mechanism in thunderstorms. *Journal of the Atmospheric Sciences, 35*(8), 1536-1548. https://doi.org/10.1175/1520-0469(1978)035<1536:REAACG>2.0.CO;2

797   Tessendorf, S. A., Wiens, K. C., & Rutledge, S. A. (2007a). Radar and lightning observations of the 3 June 2000 electrically inverted storm from STEPS. *Monthly Weather Review, 135*(11), 3665-3681. https://doi.org/10.1175/2006MWR1953.1

800   Tessendorf, S. A., Rutledge, S. A., & Wiens, K. C. (2007b). Radar and lightning observations of normal and inverted polarity multicellular storms from STEPS. *Monthly Weather Review, 135*(11), 3682-3706. https://doi.org/10.1175/2007MWR1954.1

803   Thomas, R. J., Krehbiel, P. R., Rison, W., Hunyady, S. J., Winn, W. P., Hamlin, T. and Harlin, J. (2004). Accuracy of the lightning mapping array. *Journal of Geophysical Research: Atmospheres, 109*(D14). https://doi.org/10.1029/2004JD004549

806   Tsenova, B., Mitzeva, R., & Saunders, C. (2010). Parameterization of thunderstorm charging including the cloud saturation effect. *Atmospheric Research, 96*(2-3), 356-365. https://doi.org/10.1016/j.atmosres.2009.11.010

809   van der Velde, O. A. & Montanyà, J. (2013). Asymmetries in bidirectional leader development of lightning flashes. *Journal of Geophysical Research: Atmospheres, 118*(24), 13-504. https://doi.org/10.1002/2013JD020257

812   Weiss, S. A., Rust, W. D., MacGorman, D. R., Bruning, E. C., & Krehbiel, P. R. (2008). Evolving complex electrical structures of the STEPS 25 June 2000 multicell storm. *Monthly Weather Review, 136*(2), 741-756. https://doi.org/10.1175/2007MWR2023.1

815   Wiens, K. C., Rutledge, S. A., & Tessendorf, S. A. (2005). The 29 June 2000 supercell observed during STEPS. Part II: Lightning and charge structure. *Journal of the Atmospheric Sciences, 62*(12), 4151-4177. https://doi.org/10.1175/JAS3615.1

818   Williams, E. R. (1985). Large-scale charge separation in thunderclouds. *Journal of Geophysical Research: Atmospheres, 90*(D4), 6013-6025. https://doi.org/10.1029/JD090iD04p06013

820   Williams, E. R. (1989). The tripole structure of thunderstorms. *Journal of Geophysical Research: Atmospheres, 94*(D11), 13151-13167. https://doi.org/10.1029/JD094iD11p13151

822   Williams, E. R., Zhang, R., & Rydock, J. (1991). Mixed-phase microphysics and cloud electrification. *Journal of the Atmospheric Sciences, 48*(19), 2195-2203. https://doi.org/10.1175/1520-0469(1991)048<2195:MPMACE>2.0.CO;2

825   Zheng, D., Shi, D., Zhang, Y., Zhang, Y., Lyu, W., & Meng, Q. (2019). Initial leader properties during the preliminary breakdown processes of lightning flashes and their associations with initiation positions. *Journal of Geophysical Research: Atmospheres, 124*(14), 8025-8042. https://doi.org/10.1029/2019JD030300

829   Zipser, E. J., Cecil, D. J., Liu, C., Nesbitt, S. W., & Yorty, D. P. (2006). Where are the most
830   intense thunderstorms on Earth?. *Bulletin of the American Meteorological Society, 87*(8), 1057-
831   1072. https://doi.org/10.1175/BAMS-87-8-1057